Available online at www.sciencedirect.com

ScienceDirect

Advances in Space Research 69 (2022) 737–750

ADVANCES IN SPACE RESEARCH (a COSPAR publication)

www.elsevier.com/locate/asr

Rarefied gas flow around a double-plate induced by temperature difference

Dandan Zeng [a,b], Rong Cai [b,*], Yanchu Yang [b,*]

[a] Institute of Mechanics, Chinese Academy of Sciences, Beijing 100190, China
[b] Aerospace Information Research Institute, Chinese Academy of Sciences, Beijing 100094, China

Received 15 June 2021; received in revised form 23 September 2021; accepted 25 September 2021
Available online 7 October 2021

Abstract

Radiometric phenomena are expected to be applied to lifting or propelling high-altitude aerospace craft, however, the temperature difference between both sides of the radiometric plate is too small to produce a substantial force. In this work, we proposed a double-plate structure as an alternative to the radiometric plate. The flow around the double-plate was studied for a wide range of plate temperatures, gap-to-radius ratios and Knudsen numbers with molecular kinetic theory and the direct simulation Monte Carlo (DSMC). Kinetic analysis reveals that the normalized force and heat fluxes acting on the plates could be well approximated by exponential-decay functions of the gap-to-radius ratio when the gap-to-radius ratio is smaller than 2. Pressure distributions on the plates demonstrate that the gas-plate interactions combine dynamics of rarefied flow, continuum flow and the geometrical effect. Dependences of the normalized forces and heat fluxes on *Kn*, gap distance, and plate temperatures were studied in dimensionless form and compared with those of radiometric flow. Analytical formulations were developed to evaluate the forces and heat flux acting on the double-plate quickly. The double-plate could produce a force which is larger than its weight at altitudes around 70km if the parameters were properly selected.

Keywords: Radiometric flow; Rarefied gas dynamics; Temperature difference; DSMC

1. Introduction

Thermal creep flow is one of the most important subjects in rarefied gas dynamics. The pioneering application of thermal creep flow is in the Crookes radiometer, which was invented in the 1870s by Sir William Crookes (Crookes 1874 XV; Stanhill 2019). The Crookes radiometer consists of a partially evacuated glass bulb containing a set of thin vanes mounted on a spindle. The vanes are black on one side and white on the other side. When the vane is exposed to the sunlight, the black side is hotter than the white side, which results in a radiometric force directed from the hot side to the cold side and drives the vane to rotate around the spindle. Another interesting application of thermal creep flow can be found in micro- and nano-scale tubes (Sharipov and Seleznev 1998). In rarefied flow, a solid boundary with a temperature gradient drives the gas around it with a uniform pressure from the colder end to the hotter end.

With the development of micro-electromechanical systems (MEMS) and outer space exploration, there is a growing interest in thermal creep flow (Anikin 2011; Chen et al. 2012; Ketsdever et al. 2012; Scandurra et al. 2007; Selden et al. 2009a, 2009b; Sone 2000; Taguchi and Aoki 2012, 2015; Wolfe et al. 2016). Selden et al. (2009a, 2009b) investigated the area and edge origin of the force acting on the radiometric plate in conditions of different Knudsen numbers, it was found out that the importance of edge region of

* Corresponding authors.
E-mail addresses: cairong@aircas.ac.cn (R. Cai), yangyc@aircas.ac.cn (Y. Yang).

https://doi.org/10.1016/j.asr.2021.09.034
0273-1177/

the plate increases with pressure for the force production. Taguchi and Aoki (2012) investigated the similarity in the flow structure around the edge of a very thin radiometric plate. In practice, the thermal creep phenomena can be used for gas transport in microscale devices (Akhlaghi and Roohi 2013; Andrew et al. 2017; Baier et al. 2017; Donkov et al. 2011; Lotfian and Roohi 2019; Passian et al. 2003; Shahabi et al. 2017; Sista and Bhattacharya 2014; Wang et al. 2019; Zhu and Guo 2017) and for gas detection in MEMS sensors (Strongrich and Alexeenko 2015; Baier et al. 2017; Barzegar Gerdroodbary et al. 2017, 2018a, 2018b; Hassanvand et al. 2018; Pikus et al. 2019; Lotfian and Roohi 2021). Ratchet-like periodically patterned micro-channels were designed to pump the fluid confined within it (Lotfian and Roohi 2019; Wang et al. 2019). For a specific device and flow conditions, the normalized Knudsen force generated in thermal creep flow mostly depends on the Knudsen number, and this effect could be used to distinguish gas species with different molecular diameters. In addition to the applications in microscale devices, the thermal creep phenomena can be employed to control or propel high-altitude aircraft and spacecraft with large area to mass ratios, such as solar sails, etc (Benford and Benford 2005; Duermann et al. 2013; White et al. 2013; Küpper et al. 2014; Nallapu et al. 2017; Firuzi and Gong 2018). For example, Nallapu et al. (2017) proposed the concept of a radiometric actuator recently, and they suggested that the radiometric actuators are free of jitter and could help small satellites achieve precision pointing of a few arc-seconds or less. Benford et al. (2005) proposed a vane like aero-spacecraft for the far upper atmosphere supported by a radiometric force with the bottom surface heated by microwave. The aero-spacecraft was supposed to hover at an altitude around 70 km, which was about 20 km higher than the highest altitude aerostats in record (“Ultra-Thin-Film Balloon Reached the Highest Altitude” 2002; Rainwater et al. November 2003; Rainwater and Smith 2004). The bottom surface of the vane was designed to be heated by microwaves to a temperature higher than 1000 K, and the vane was envisioned to be made of an ultra-light carbon material that could sustain a large temperature difference between the two sides. Cornella et al. (2012) analyzed the propulsion that could be provided by multi-vane radiometer arrays, which were mounted on a near-space airship to withstand wind disturbances. They further studied the impact of the separation distance and vane thickness on the force experimentally and numerically (Cornella et al. 2011; Ventura et al. 2013).

Even though many efforts have been made to apply radiometric forces to aerospace technology, two theoretical factors impede its practical use in space and near-space craft. First, the required diameter of the radiometric plate is thought to be around ten times the molecular mean free path (Lu 2005; Selden et al. 2009a,b). As an example, at an altitude of 80 km, the mean free path is about 5 mm (USSA 1976) and diameter of the designed radiometric plate is around 50 mm. It is impossible for such a small plate to carry a practical payload. To solve the problem of the size limitation, a porous plate might be considered, as studied in Ref. (Passian et al. 2003; Duermann et al. 2013; Küpper et al. 2014) Second, the thermal conduction inside the plate leads to a temperature difference of several tens of Kelvin between both sides, which is so small that the induced radiometric force can barely lift the plate itself (Cornella et al. 2012; Ventura et al. 2013). As analyzed by Cornella et al. (2012), a coated aerogel plate operating at 60 km with a thickness of 0.64 mm and side length of 1.5 mm could maintain a temperature difference of 20 K and provide a thrust of 0.231 μN.However, the weight of the plate itself was about 1.81 μN, which was 7.8 times the thrust. To produce a force that is larger than the weight of the plate, a temperature difference of more than 100 K is essential for a regular material with completely diffusive surfaces, as discussed in our previous work (Zeng et al. 2020). To maintain a large temperature difference, increasing the thickness of the plate could be a choice, however, larger thickness brings larger weight, which could be a negative factor for aerospace technology. In this work, we proposed a double-plate structure as an alternative solution to the problem. As shown in Fig. 1, the double-plate is constructed of a colder plate and a hotter plate, and the temperature is uniform throughout each plate, and the temperature of one plate is much higher than the other. When the gap distance between the two plates converges to zero, the double-plate reduces to a radiometric plate. For purpose of generality, we refer to the flow around the double-plate as Knudsen flow and the force acting on both plates as the Knudsen force. Heat transfers between the plates by thermal radiation and gas-surface interactions, and they are much less efficient than the thermal conduction through a condensed material. Furthermore, the rate of thermal radiation can be reduced by tuning the radiative parameters of the plates. Therefore, a large temperature difference between the plates could be obtained, and then a sufficiently large Knudsen force might be produced.

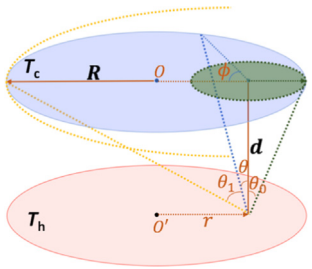

Fig. 1. (Color online) A double-plate with gap distance d and radius R. θ is the incident angle of a molecule impinging on the internal surface at a radius of r. θ is divided into three intervals by $\theta = \theta_0$ (the green dotted circle) and $\theta = \theta_1$ (the yellow dotted curve). (For interpretation of the references to color in this figure legend, the reader is referred to the web version of this article.)

To evaluate the gas dynamics of the double-plate structure, we studied the flow around a thin, circular double-plate in near-space in this work. First, we analyzed the problem by kinetic theory and scaled it by dimensional analysis. Then, we simulated the flow with DSMC for a wide range of temperature, gap distance, and plate size. Emphasis was put on the mechanism of the flow, force production and the heat transferring by gas-surface interactions. We hope that the presented results will be useful for understanding the rarefied flow around the double-plate and applications of rarefied phenomena in near-space and space technology.

2. Theoretical analysis

The double-plate consists of two parallel circular plates. The plates are very thin, and the thickness was set to zero. The radius of the plates was denoted by R, and the distance between the two plates was denoted by d, as shown in Fig. 1. The temperatures of the colder upper plate and the hotter lower plate were denoted by T_c and T_h, respectively. The surfaces of the both sides are assumed to be completely diffusive. The double-plate is immersed in an atmosphere with temperature T_0, pressure p_0, mean free path λ_0, and molecular mass m_g. The dependence of the gaseous viscosity μ_0 with temperature T_0 can be described as follows: $\mu_0 \propto T_0^w$. μ_0 can be calculated using the aforementioned gas parameters through kinetic theory (Bird 1994). The value of w is associated with the gas species. In this work, value of w was fixed at 0.75, which is an intermediate value for common gas species. Monatomic molecule is used for purpose of simplification.

Let B denote the Knudsen pressure, which is defined as the Knudsen force acting on the double-plate divided by its cross-sectional area (πR^2). B can be written as a function of the above parameters, i.e.,

$$B = b\left(T_c, T_h, T_0, p_0, \lambda_0, R, d, m_g\right) \tag{1}$$

Similarly, the rate of heat transferring between the gas and the double-plate, which is denoted by H, can be written as

$$H = h\left(T_c, T_h, T_0, p_0, \lambda_0, R, d, m_g\right) \tag{2}$$

The Knudsen pressure and energy flux acting on the double-plate in free molecular flow are denoted byB^F and H^F respectively. According to dimensional analysis, Eq. (1) can be written as

$$\frac{B}{B^F} = \mathcal{B}\left(\frac{T_c}{T_0}, \frac{T_h}{T_0}, \frac{d}{R}, Kn\right) \tag{3}$$

and Eq. (2) can be written as

$$\frac{H}{H^F} = \mathcal{H}\left(\frac{T_c}{T_0}, \frac{T_h}{T_0}, \frac{d}{R}, Kn\right) \tag{4}$$

The values of B^F and H^F can be obtained by summing those on each surface of both plates. Let "h.l.", "h.u.","c .l." and "c.u." denote the lower surface of the hotter plate, the upper surface of the hotter plate, the lower surface of the colder plate and the upper surface of the colder plate respectively. It is easy to obtain the pressure and energy flux acting on the external surfaces (i.e., the "h.l." surface and the "c.u." surface) according to the kinetic theory (Bird 1994). Specifically, $B^F_{c.u.} = \frac{p_0}{2}\left(1 + \sqrt{T_c/T_0}\right)$, $B^F_{h.l.} = \frac{p_0}{2}\left(1 + \sqrt{T_h/T_0}\right)$, $H^F_{c.u.} = \frac{c_0 p_0}{2}(1 - T_c/T_0)$, $H^F_{h.l.} = \frac{c_0 p_0}{2}(1 - T_h/T_0)$, where c_0 is the expected velocity of the molecules, which can be calculated by $c_0 = \sqrt{8k_B T_0/\pi m_g}$. The interactions between the gas and the internal surfaces (i.e., the "h.l." surface and the "c.u." surface) are a little more complicated. Fig. 1 shows that molecules impinges on the internal surface at a radius of r could be divided into 3 categories on the basis of the incident angle θ. When $\theta < \theta_0$, the incident molecules definitely come from the surface at face-to-face; when $\theta_0 < \theta < \theta_1$, a ϕ/π portion of the molecules come from the surface at face-to-face, and $1 - \phi/\pi$ portion of the molecules came from the environment; when $\theta > \theta_1$, the incident molecules definitely come from the environment. The portion of molecules impinging on the internal surfaces and coming from the environment determines the reduction of the Knudsen force caused by the gap distance. The values of θ_0, θ_1 and ϕ can be calculated by

$$\tan\theta_0 = (R - r)/d \tag{5}$$

$$\tan\theta_1 = (R + r)/d \tag{6}$$

$$\cos\phi = \frac{d^2\tan^2\theta + r^2 - R^2}{2rd\tan\theta} \tag{7}$$

Integrating all the molecules acting on the surface, one can obtain the Knudsen pressure in free molecular flow acting on upper surface of the hotter plate as

$$B^F_{h.u.} = \frac{p_0\left(\sqrt{T_h/T_0} + \sqrt{T_c/T_0}\right)}{2} + \frac{p_0\left(\sqrt{T_c/T_0} - 1\right)}{2} \times \int_0^1 2r'\left[-\cos^3\theta_0 + \frac{3}{\pi}\int_{\theta_0}^{\theta_1}\phi\cos^2\theta\sin\theta\,d\theta\right]dr' \tag{8}$$

with $r' = r/R$. Similarly, the rate of heat flux acting on the upper surface of the hotter plate can be written as

$$H^F_{h.u.} = \frac{c_0 p_0}{2}\left(\frac{T_c}{T_0} - 1\right)\int_0^1 2\left[\sin^2\theta_0 + \int_{\theta_0}^{\theta_1}\frac{\phi\sin 2\theta}{\pi}d\theta\right]r'dr' + \frac{c_0 p_0}{2}\left(1 - \frac{T_h}{T_0}\right) \tag{9}$$

Swapping the subscript of 'h' and 'c' in Eq. (8) and Eq. (9), we could obtain $B^F_{c.l.}$ and $H^F_{h.u.}$. Then the pressure acting on the double-plate by summing $B^F_{h.l.}$, $B^F_{h.l.}$, $B^F_{c.l.}$ and $B^F_{c.u.}$ as

$$\frac{B^{\mathrm{F}}}{B_0^{\mathrm{F}}}=\int_0^1 6\left(\frac{1-\cos^3\theta_0}{3}+\int_{\theta_0}^{\theta_1}\frac{\phi\cos^2\theta\sin\theta}{\pi}\mathrm{d}\theta\right)r'\mathrm{d}r' \tag{10}$$

with $B_0^{\mathrm{F}}=\frac{p_0\sqrt{T_{\mathrm{h}}/T_0}-\sqrt{T_{\mathrm{c}}/T_0}}{2}$ corresponding to the Knudsen pressure acting on the double-plate in the limit of zero gap distance, or on a radiometric plate with the temperatures of the hotter side and the colder side equaling to T_{h} and T_{c} respectively.

Similarly, the energy flux transferring to the double-plate can be obtained as

$$\frac{H^{\mathrm{F}}}{H_0^{\mathrm{F}}}=1+\int_0^1 2\left(\cos^2\theta_0-\int_{\theta_0}^{\theta_1}\frac{\phi\sin2\theta}{\pi}\mathrm{d}\theta\right)r'\mathrm{d}r' \tag{11}$$

with $H_0^{\mathrm{F}}=\frac{c_0p_0}{2}\left(2-\frac{T_{\mathrm{h}}}{T_0}-\frac{T_{\mathrm{c}}}{T_0}\right)$. In the limit of $d/R\to 0$, $\theta_0=\theta_1=\pi/2$ for any r', thus $B^{\mathrm{F}}/B_0^{\mathrm{F}}=1$ and $H^{\mathrm{F}}/H_0^{\mathrm{F}}=1$ are obtained. In the limit of $d/R\to+\infty$, $\theta_0=\theta_1=0$ for any r', $B^{\mathrm{F}}/B_0^{\mathrm{F}}=0$ and $H^{\mathrm{F}}/H_0^{\mathrm{F}}=2$ are obtained. Because θ_0, θ_1 and ϕ are functions of r' and d/R, $B^{\mathrm{F}}/B_0^{\mathrm{F}}$ and $H^{\mathrm{F}}/H_0^{\mathrm{F}}$ depend only on d/R. According to Eq. (10) and (11), variations of $B^{\mathrm{F}}/B_0^{\mathrm{F}}$ and $H^{\mathrm{F}}/H_0^{\mathrm{F}}$ withd/R can be obtained, as displayed in Fig. 2. It is shown that the dependence of$B^{\mathrm{F}}/B_0^{\mathrm{F}}$ on d/R can be well approximated by $B_{\mathrm{F}}/B_{\mathrm{F}}^0=\exp(-0.724d/R)$, and $H^{\mathrm{F}}/H_0^{\mathrm{F}}$ can be well approximated by $H^{\mathrm{F}}/H_0^{\mathrm{F}}=2-\exp(-d/R)$ for $d/R\le 2$. The largest relative deviation between the theoretical value and the approximated value is about 1% when $d/R\le 2$.

By summing $B_{\mathrm{h.u.}}^{\mathrm{F}}$ with $B_{\mathrm{h.l.}}^{\mathrm{F}}$, one can obtain the pressure acting on the hotter plate in free molecular flow, which is denoted by $B_{\mathrm{h}}^{\mathrm{F}}$, as

$$\frac{B_{\mathrm{h}}^{\mathrm{F}}}{B^{\mathrm{F}}}=\frac{\sqrt{T_0}-\sqrt{T_{\mathrm{c}}}}{\sqrt{T_{\mathrm{h}}}-\sqrt{T_{\mathrm{c}}}} \tag{12}$$

Similarly, the pressure acting on the colder plate in the free molecular flow, which is denoted by $B_{\mathrm{c}}^{\mathrm{F}}$ satisfies

$$\frac{B_{\mathrm{c}}^{\mathrm{F}}}{B^{\mathrm{F}}}=\frac{\sqrt{T_{\mathrm{h}}}-\sqrt{T_0}}{\sqrt{T_{\mathrm{h}}}-\sqrt{T_{\mathrm{c}}}} \tag{13}$$

Equations (12)−(15) are applicable to any temperatures and gap distance. Besides, Eq. (12) and (13) show that the colder plate experiences an upward force and the hotter plate experiences a downward force in free molecular flow if the plate temperatures satisfy the inequality$T_{\mathrm{h}}>T_{\mathrm{c}}>T_0$.Therefore, the plates seemed to interact repulsively, which allows them to be connected by light, flexible materials.

3. Numerical details

The flow in transitional regime was investigated by direct simulation Monte Carlo (DSMC) (Bird 1994). DSMC is a molecular-based algorithm to solve the Boltzmann equation, and it is applicable to the range of flow regimes from free molecule to continuum (Roohi and Darbandi 2012; Goshayeshi et al. 2015; Roohi and Stefanov 2016). The fundamental idea of DSMC is that the kinetics of the molecules can be split into two uncoupled parts—intermolecular collisions and free molecular motions—when the time interval is much smaller than the mean collision time. In the present simulations, the collisions between the molecules were simulated using the variable hard sphere collision model. The collision pair was selected according to the no time count method (Bird 1994).

Fig. 3 illustrates the computational setup. The flow field around the circular plates was axially symmtric, thereofore, the algorithm for axisymmetric flow was used to solve the problem. The hot plate was placed at $z=0$, which was at the middle height of the domain, while the cold plate was placed at $z=d$. The domain had height D in the z-direction and length $D/2$ in the r-direction. On the plate surfaces, molecules reflected diffusively with velocities sampled from a Maxwellian velocity distribution function at the surface temperature. At $r=0$, axial symmetry was applied. Molecules moved in and out of the domain through the boundary at $r=D/2$ and $z=\pm D/2$, where the boundary condition was set the same as the environment.

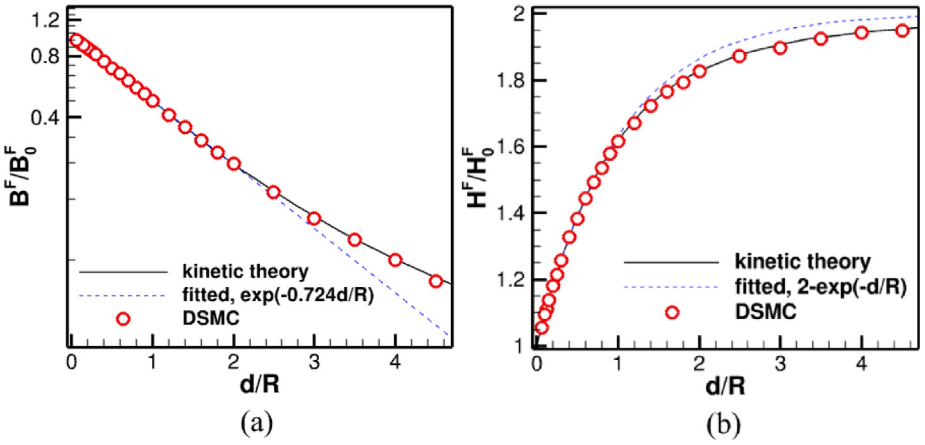

Fig. 2. Dependences of normalized Knudsen pressure (a) and heat flux (b) on gap distance d/R in the limit of free molecular flow.

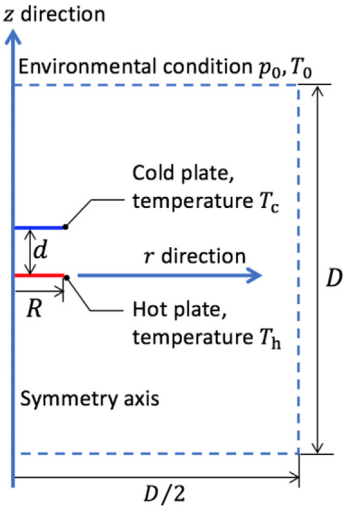

Fig. 3. (Color online) The axisymmetric model and coordination system used in this work.

For the present simulations,$T_0 = 197$K and$p_0 = 1.05$Pa, which correspond to the atmospheric conditions at an altitude of 80 km according to US Standard Atmosphere (1976). In this work, we changed the values of the dimensionless quantities of T_c/T_0, T_h/T_0, Kn, and d/R by changing T_c, T_h, R, and d. We ran a number of simulations for various operating conditions (various $T_c/T_0, T_h/T_0, Kn, d/R$). Three sets of surface temperatures were used, $(T_c/T_0, T_h/T_0) = (1, 1.68)$, $(1.52, 3.05)$, and $(3.05, 8.12)$. T_h/T_0 =1.68, 3.05, and 8.12 correspond to plate temperatures of 331, 600, and 1600 K, respectively, which are well below the melting temperature of the polythene membrane, polyimide aerogel, and carbon aerogel, respectively. These materials have potentials for manufacturing the presented structure due to their low densities, high mechanical strengths and high-temperature stabilities. The temperature of the colder plate could be as high as 600 K ($T_c/T_0 = 3.05$) for $T_h/T_0 = 8.12$ due to the very high temperature of the hotter side and the effect of thermal transfer by radiation. The radius-based Kn values were set to 0.1, 0.25, 0.5, 1.0, 2.0. The value of d/R ranged from 0.25 to 1. At the initial time, the gas was set to be quiescent and in thermodynamic equilibrium with the environment. After the flow evolved for a sufficiently long time and reached a steady state, the quantities of interest were sampled and averaged for time steps to achieve acceptable statistical accuracy.

Prior to the simulations, the convergence of the flow for the computational domain size, temporal and spatial discretization, and the number of molecules used in one cell were examined to guarantee the reliability of the presented results. The linear size of the cell was denoted as Δl, and the time step was denoted as Δt. We set $\alpha = \Delta l/\lambda_0 = \Delta t/\tau_0$, where τ_0 is the mean collision time in the environmental condition. The number of simulation molecules per cell was denoted by N_c. In this work, we set $D/R = 40$, $\alpha = \min(0.5, 0.5d/\lambda_0)$, and $N_c \geq 20, 40, 60$ for $(T_c/T_0, T_h/T_0) = (1, 1.68)$, $(1.52, 3.05)$, $(3.05, 8.12)$ respectively. The convergency of the simulation with D, α, and N_c were tested and is shown in Tab.1. In Tab. 1, ε was double the value of a statistical standard deviation, and it was used to evaluate the statistical scatter of the sampled quantities in this work. Table 1 shows that the relative deviation caused by numerical discretization was less than or equal to about 2% for the chosen D,α andN_c.

Fig. 2 compares the simulated Knudsen pressure for free molecular flow with theoretical values. Both results are consistent, which further validates the program used in this work.

4. Results and discussions

4.1. Flow field

Fig. 4 shows the flow structure of the gas around the plates with $Kn = 0.25$,$d/R = 1$, $T_c/T_0 = 3.05$ and

Table 1
Variation of computed B with computational domain size, spatial and temporal discretization and number of molecules used in one cell under conditions of.$Kn = 0.5$

	D/R	α	N_c	B/B_F	ε/B_F
$T_c/T_0 = 1T_h/T_0 = 1.68d/R = 0.25$	40	0.25	20	0.467	0.009
	40	0.25	100	0.469	0.009
$T_c/T_0 = 1.52T_h/T_0 = 3.05d/R = 0.25$	40	0.0625	40	0.529	0.0097
	40	0.25	40	0.527	0.0071
	40	0.125	100	0.521	0.0044
	80	0.25	40	0.522	0.0075
	40	0.5	40	0.537	0.0079
$T_c/T_0 = 3.05T_h/T_0 = 8.12d/R = 0.25$	40	0.125	60	0.588	0.0029
	40	0.125	100	0.589	0.0027
	40	0.25	60	0.586	0.0043
	80	0.25	60	0.578	0.0026
	40	0.5	60	0.597	0.0051
$T_c/T_0 = 1.52T_h/T_0 = 3.05d/R = 0.5$	40	0.0625	40	0.520	0.0069
	40	0.25	40	0.527	0.0079
	40	0.5	40	0.533	0.0074
	80	0.5	40	0.527	0.011

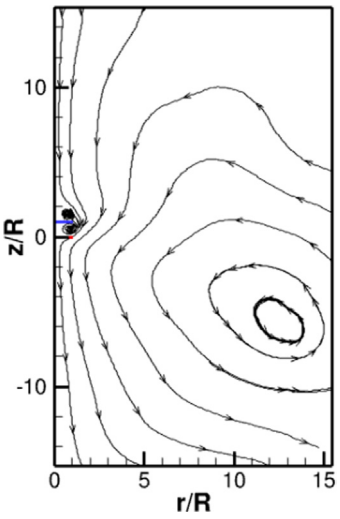

Fig. 4. (Color online) Streamlines for $Kn = 0.25$, $d/R = 1$, $T_c/T_0 = 3.05$, and $T_h/T_0 = 8.12$.

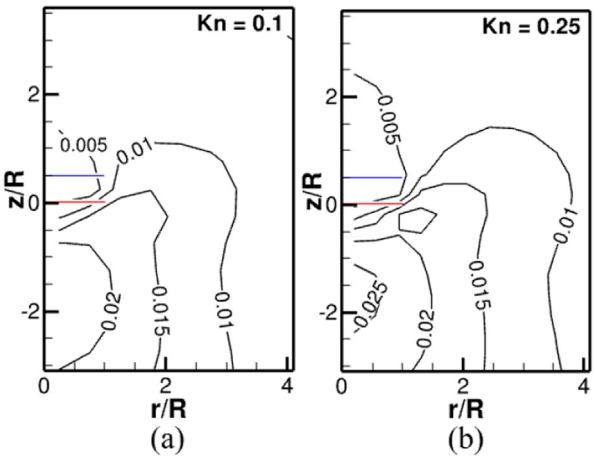

Fig. 6. (Color online) Isolines of the normalized momentum magnitude ($\rho v/\rho_0 c_0$) around the plates for $Kn = 0.1$ (a), 0.25 (b) in conditions of $d/R = 0.5$, $T_c/T_0 = 3.05$, and$T_h/T_0 = 8.12$.

$T_h/T_0 = 8.12$. The temperature difference induced a downward flux, which produces a large vortex located far away from the double-plate, as shown in Fig. 4. The downward flux induces a small vortex formed above the colder plate, and a vortex formed between both plates. Generally, the flow structure is similar to the flow around a radiometric plate except that a vortex formed between the plates which is absent in the radiometric flow.

Fig. 5 demonstrates the effects of Knudsen number on flow structure and velocity magnitude around the double plate. The velocity magnitude in these figures were scaled by c_0. Fig. 5 shows that the velocity magnitude was larger for smaller Kn, this phenomenon pertained to the stronger synergetic effectwhile weaker dissipation effect of the molecular motion at smaller Knudsen numbers. Though the velocity magnitude increases with decreasing Kn, the magnitude of momentum flux decreases with Kn as shown in Fig. 6, this indicates a decreasing normalized force with decreasingKn as expected. The vortex above the colder plate is similar with that above the colder surface of a radiometric plate (Zeng et al. 2020), and the size of the vortex generally increased with the Knudsen number. The vortex motions between the plates were governed by the gap-to radius ratio and Kn.

Fig. 7 shows the effects of gap distance on the flow. The size of the vortex above the colder plate and the normalized velocity generally decreased with the gap distance. The size of the vortex between the plates increased with d/R; Fig. 7 (a) shows that the vortex between the double-plate disappears because the gap distance is smaller than the local mean molular free path. Both Fig. 5 and Fig. 7 demonstrate that there are two regions of maximum velocity for all the simulated cases: one near the edge of the hotter plate and the other a distance about R below the center of the hotter plate.

4.2. Pressure distribution on plates

The pressure acting on the surfaces were calculated by the momentum change between the incident and reflected

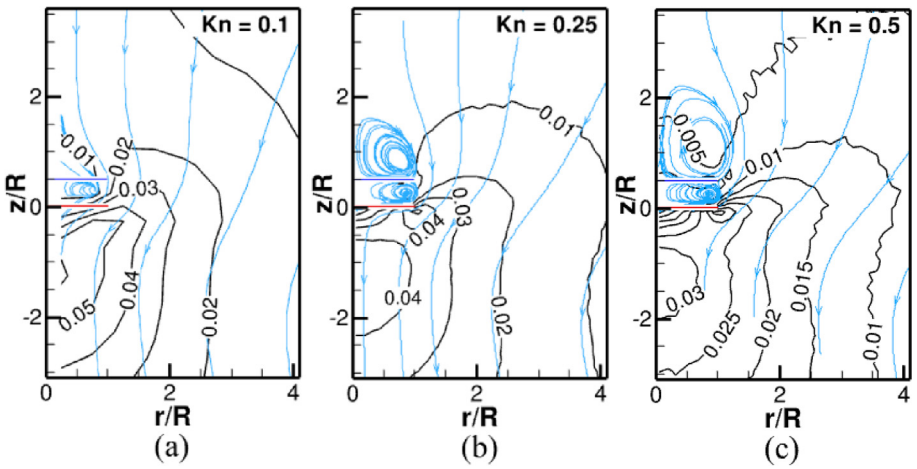

Fig. 5. (Color online) Isolines of the normalized velocity magnitude and streamlines around the plates for $Kn = 0.1$ (a), 0.25 (b), 0.5 (c) in conditions of $d/R = 0.5$, $T_c/T_0 = 3.05$, and$T_h/T_0 = 8.12$.

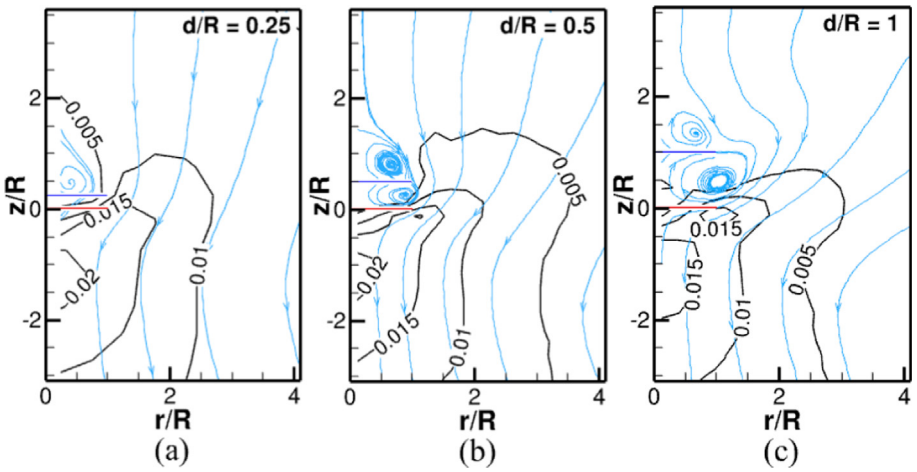

Fig.7. (Color online) Effect of gap distance on the flow structure and velocity field around the plates: Kn= 0.5,$T_c/T_0 = 1.52$, and$T_h/T_0 = 3.05$. Insets: corresponding overall flow around the plates.

molecules. In this work, we denote the pressure on the surfaces (or plates) at r by P_a, and denote the averaged pressure acting on the surfaces (or plates) by B_a, where subscript "a" could be "h.l.", "h.u.","c.l.","c.u.","h" and "c". To unmask the mechanism underlying Eq. (3) we studied the distributions of pressure along the radius-direction acting on each surface. In free molecular flow, the pressure acting on the external surfaces is uniform along the $r-$direction; as for the internal surfaces of the double-plate, more molecules come from the face-to-face surface and impinge on the central region, and these molecules carry larger momentum than those from the environment, which result in a larger force acting on the central region than on the edge. Fig. 8 demonstrates that magnitude of the pressure acting on internal surfaces and the double-plate decreases gently with r/R in the range of $(0, 1-d/R)$, and decreases steeply with r/R in the range of $(1-d/R, 1)$.

Fig. 9 displays the effects of Kn on pressure distributions in conditions of $T_c/T_0 = 1.52$ and $T_h/T_0 = 3.05$. In these figures, the pressures are normalized by those in free molecular flow and r is normalized by R.

Fig. 9 (a-c) shows the pressure distributions on the external surfaces. It is seen that magnitudes of the normalized pressures on these surfaces decreases with decreasing Kn as expected. Besides, the pressures acting on the external surfaces increase with r, especially for smaller Knudsen numbers, which can be explained by the stronger rarefied gas effect on the edge region than on the central region, as illustrated in Fig. 10. Pressure distributions on the internal surfaces are displayed in Fig. 9 (d-f). It is obvious that magnitudes of the normalized pressures on the internal surfaces decrease with decreasing Kn. Fig. 9 (d-e) shows that the similarity in pressure distributions of the "h.u." and "c.l." surface in free molecular flow (as shown in Fig. 8) is broken down by the downward mainstream in transitional flow. Fig. 9 (d) demonstrates that magnitude of $p_{h.u.}$ increases with r in the edge region for smaller Knudsen numbers of 0.25 and 0.1, this is quite different from the ocassions in free molecular flow (Fig. 8a) and for a large Kn of 0.5 (Fig. 9d) that the magnitude of $p_{h.u.}$ decreases with r. The larger $p_{h.u.}$ near the edge region than that in the central region for a small Knudsen number is caused by the downward mainstream, which carries more molecules impinging on the edge region with an extra momentum. The mechanism was further depicted in Fig. 10. When the Knudsen number is small, the stream imposes

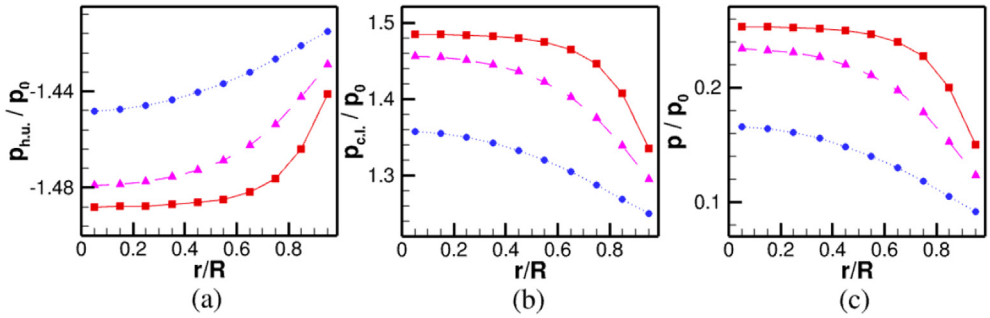

Fig. 8. (Color online) Distributions of pressure on the upper surface of the hotter plate (a), the lower surface of the colder plate (b) and double-plate (c) in free molecular flow for $d/R = 0.25$ (blue-dot), 0.5 (magenta-dashed), 1 (red-solid) in conditions of $T_c/T_0 = 1.52$ and$T_h/T_0 = 3.05$. (For interpretation of the references to color in this figure legend, the reader is referred to the web version of this article.)

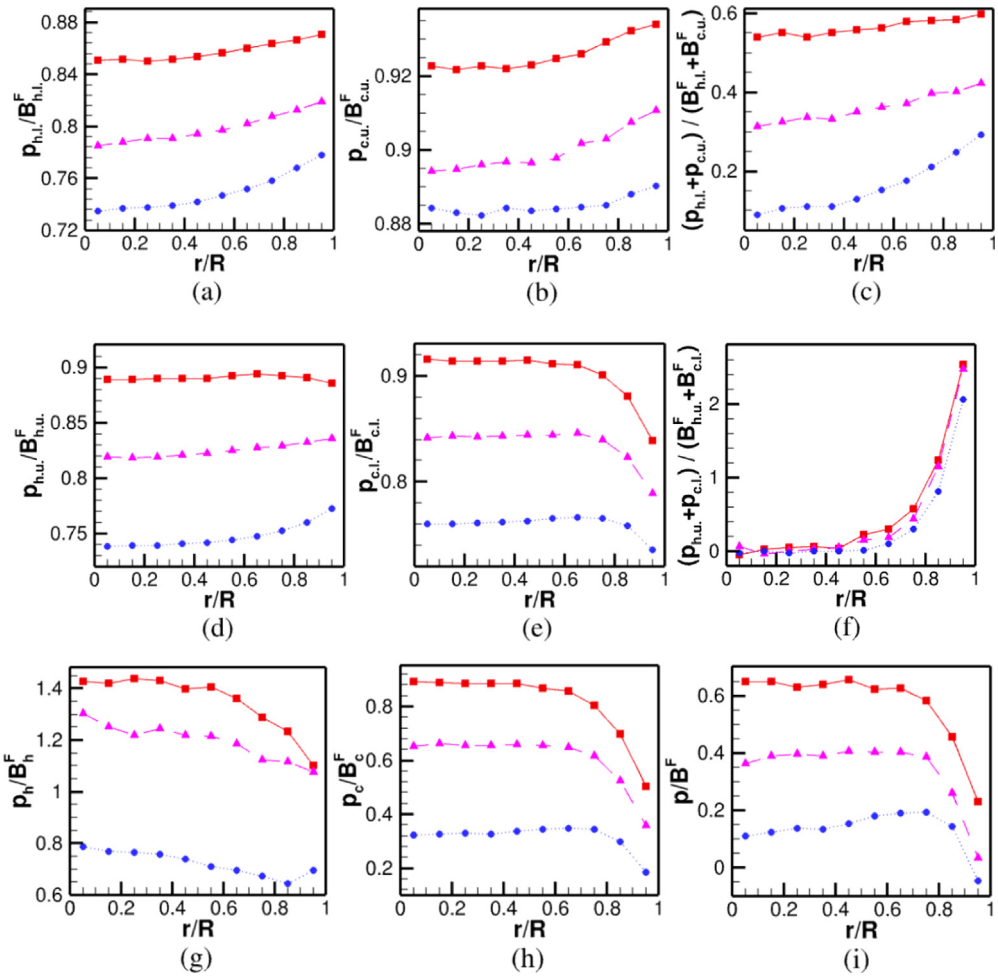

Fig. 9. (Color online) Distributions of pressure on the surfaces (a) lower surface of the hotter plate, (b) upper surface of the colder plate, (c) the external surfaces, (d) upper surface of the hotter plate, (e) lower surface of the colder plate, (f) the internal surfaces, (g) the hotter plate, (h) the colder plate, (i) the double-plate, with $Kn = 0.1$ (blue-dot), 0.25 (magenta-dashed), and 0.5 (red-solid) in conditions of $d/R = 0.25$, $T_c/T_0 = 1.52$ and$T_h/T_0 = 3.05$. (For interpretation of the references to color in this figure legend, the reader is referred to the web version of this article.)

an extra pressure near the edge of the h.u. surface, which conceals the pressure distribution discipline in free molecular flow. On the contrary, the $p_{c.l.}$ decreases steeply with r in the range of $1 - d/R < r/R < 1$ for all the studied cases, which is qualitatively consitent with the that in free molecular flow. In the range of $0 < r/R < 1 - d/R$, the variation of $p_{c.l.}$ with r depends on the gap-to-radius ratio and the Knudsen number. For small Knudsen numbers and gap-to radius ratios such as $Kn = 0.1$ and $d/R = 0.25$, $p_{c.l.}/B^F_{c.l.}$ reaches a maximum value of 0.77 between $r/R = 0.65 - 0.75$. As for larger Knudsen numbers or larger gap distances,$p_{c.l.}$ varies little along the $r-$direction in the range of $0 < r/R < 1 - d/R$. From the above discussion, we might come to the conclusion that the effect of Knudsen number and the downward mainstream dominate the distributions of $p_{h.u.}$, while the Knudsen number and the gap distance dominate the distributions of $p_{c.l.}$. Fig. 9 (f) shows that distributions of normalized "$p_{h.u.} + p_{c.l.}$" are similar for different Kn when the gap distance is fixed, and the magnitude of "$p_{h.u.} + p_{c.l.}$" increases with increasing Kn. Fig. 9(f) also demonstrates that the magnitude of the summed pressure acting on the internal surfaces increases with r monotonically.

The pressure acting on the hotter plate and colder plate are denoted by p_h and p_c respectively. Specifically, $p_h = p_{h.l.} + p_{h.u.}$, $p_c = p_{c.l.} + p_{c.u.}$. The pressure acting on the double plate is denoted by p, and $p = p_h + p_c$. For larger Kn such as 0.5 and 0.25, the magnitude of the downward p_h decreases monotonically with r due to the larger upward $p_{h.l.}$ near the edge region; however, when the Kn reduces to 0.1, the effect of $p_{h.u.}$ overwhelms $p_{h.l.}$ near the edge region, thus the magnitude of p_h increase with r near the edge of plate, as shown in Fig. 9 (g). Fig. 9(h) illustrates that the distributions of pressure acting on the colder plate are similar with that on its lower surface. Fig. 9(i) shows that the variations of pressure along the $r-$direction depend on Kn. The distributions of p are similar with that in the free molecular flow when Kn is larger than 0.25; however, when Kn reduces to 0.1, the pressure increase with increasing r due to the stronger continuum effect in the cen-

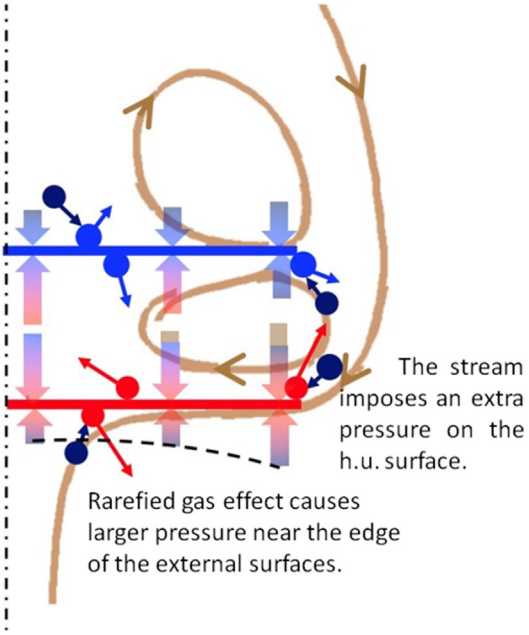

Fig. 10. (Color online) Schematic of flow mechanism. Symbols represent gas molecules coming from the environment (dark blue), the colder plate (blue) and hotter plate (red). The gradient arrows represent pressures acting on the surfaces. Brown lines represent the streams. (For interpretation of the references to color in this figure legend, the reader is referred to the web version of this article.)

tral region, this effect is concealed by the larger downward pressures acting on the internal surfaces near the edge region, which causes a decreasing pressure near the edge region; furthermore, when *Kn* equals to 0.1, the interaction between the downward mainstream and the edge region of the double-plate overwhelms other effects and produces a negative pressure at the edge region, as displayed in Fig. 9(i).

According to the above analysis, we could say that the pressure acting on the double-plate is a combined effect of rarefied gas flow, the interaction between the mainstream and plates, and the geometric characteristic of the double-plate, i.e. the gap-to-radius ratio.

4.3. Forces acting on plates

The normalized pressures acting on the colder and hotter plates for different plate temperatures are plotted as functions of *Kn* in Fig. 11. In these figures, the pressures are scaled with those values in free molecular flow, and the error bars are double the standard deviation. The results of B_h/B_h^F for $T_c/T_0 = 1$ and $T_h/T_0 = 1.68$ are not displayed because of the zero value of B_h^F.

Fig. 11 demonstrates that the normalized pressures tend to be 1 for large *Kn*, and to be 0 for small *Kn*, as expected. It can be seen that the normalized pressure acting on the colder plate increased monotonically with *Kn*; however, the magnitude of the normalized pressure acting on the hotter plate reached its maximum value at an intermediate *Kn*. This could be explained as follows: the downward flux, which were absent in the free molecular flow, carried molecules towards the edge region of the hotter plate and resulted in an additional downward force on it, as demonstrated by Fig. 9(d) and shown in Fig. 10, therefore, a maximum normalized pressure larger than 1 at an intermediate *Kn* was obtained; the same flux carried molecules away from the colder plate and decreased the upward force acting on it; however, this effect was consistent with the generally decreasing force with decreasing *Kn* for the colder plate, therefore, a monotonically decreasing pressure with *Kn* on the colder plate was obtained. The impacts of the gap distance on the normalized pressures are generally consistent for different plate temperatures and *Kn*. The gap distance determines the thinness of the gas between the plates. The smaller the gap is, the more the gas in the gap flows like free molecules, therefore, the larger the normalized pressure acting on each plate is. The plate temperatures

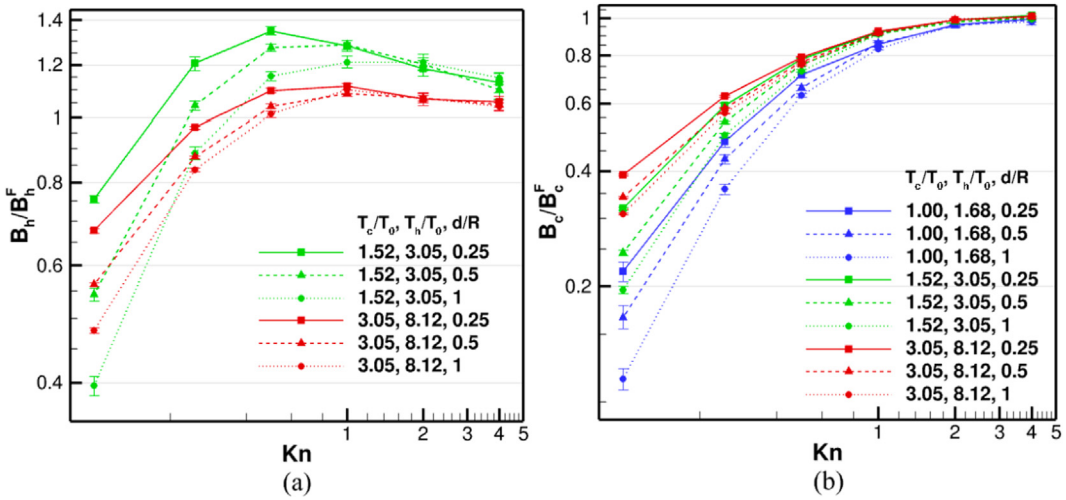

Fig. 11. (Color online) Knudsen pressures acting on the hotter plate (a) and the colder plate (b) normalized by those in free molecular flow versus *Kn* for different plate temperatures and d/R.

also have great influences on the normalized pressure, especially for small Knudsen numbers. In particular, the higher the plate temperatures are, the larger the normalized pressure acting on the colder plate is. This phenomenon is caused by the expansion effect of the plates, i.e., higher plate temperatures result in larger local Kn values corresponding to larger normalized pressures.

The pressure acting on the double-plate, which was normalized by B_F, was calculated by summing the pressures acting on each plate. Values of B_F for different plate temperatures and d/R can be calculated using Eq. (3) and (9). Though the gap-to-radius ratio imposes a strong influence on the scaled pressure acting on each plate (Fig. 11), its influence on the normalized pressure acting on the double-plate is much weaker, as shown in Fig. 12. Table 2 lists the normalized pressure B/B_F simulated for $d/R = 0.25, 0.5, 1.0$.It is shown in Fig. 12 and Tab. 2 that the influences of plate temperature and gap distance on the normalized pressure depend on Kn. When $Kn \geq 1$, the plate temperatures have a weak impact on the normalized pressure. For example, when $Kn = 1$ and $d/R = 0.25$, the value of B/B_F for $(T_c/T_0, T_h/T_0) = (3.05, 8.12)$ was 11% larger than that for $(T_c/T_0, T_h/T_0) = (1, 1.68)$; however, when Kn decreased to 0.1, the difference increased to 112%.This phenomenon in the summed pressure was similar to the pressure acting on each plate, and it could also be explained by the larger local Knudsen number caused by the higher plate temperatures for small Knudsen numbers. Fig. 13 shows that the normalized pressure acting on the double-plate can be approximated by $B/B^F = 2Kn_e^{1.25}/\left(1 + 2Kn_e^{1.25}\right)$ with $Kn_e = Kn\left(1 + \frac{T_c/T_0 + T_h/T_0 - 2}{9\left(1+Kn^2\right)}e^{-Kn}\right)$ in the range of Kn studied in this work. This formulation could be used to evaluate the force acting on the double-plate quickly. Due to the weaker effect of gap distance on B/B^F, the formulations are the same with that obtained for the radiometric plate in our previous work (Zeng et al. 2020).

Because the double-plate studied in this work is axis-symmetrical, the shear force acting on it equals to 0 N. The pressure force acting on the double-plate can be calculated by multiplying the pressure by πR^2. For a specific double-plate with a fixed radius and gap distance, the force acting on it depends on the plate temperatures, including T_c and T_h, and the environmental conditions parameterized by T_0, p_0, and λ_0. The values of T_0, p_0, and λ_0 are primarily determined by the operating altitude of the double-plate. Herein, the environmental parameters were extracted from the US Standard Atmosphere (1976). The gross force provided by the double-plate increased with decreasing gap distance, therefore, we set the gap distance to be $d = 0.25R$ to obtain a larger force. The radius of the double-plate was primarily determined by the operating altitude, assuming that the maximum force occurs at a constant Knudsen number. As an example, we studied the force provided by the double-plate with a radius of 0.5 cm considering the mean free molecular path for an altitude of 60–80 km. Fig. 14 illustrates the force produced by the double-plate with a radius of 0.5 cm versus altitude for different plate

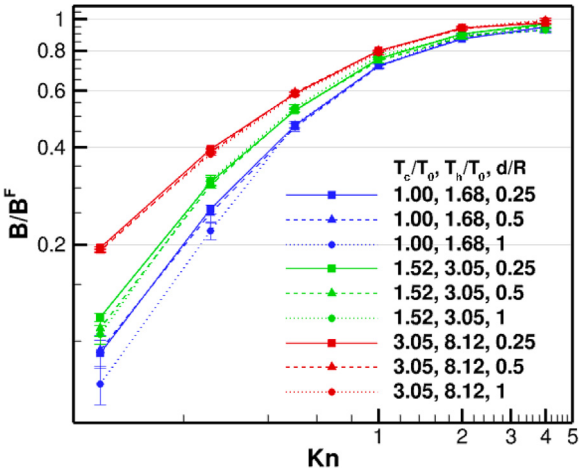

Fig. 12. (Color online) Pressures acting on the double-plate normalized by those in free molecular flow versus Kn for different plate temperatures and d/R.

Table 2
Simulated B/B_F for all the studied cases.

$\left(\frac{T_c}{T_0}, \frac{T_h}{T_0}\right)$	d/R	Kn					
		4	2	1	0.5	0.25	0.1
(1, 1.68)	0.25	0.948	0.872	0.718	0.467	0.257	0.0919
	0.5	0.929	0.879	0.715	0.462	0.250	0.0939
	1.0	0.926	0.893	0.718	0.471	0.220	0.0737
(1.52, 3.05)	0.25	0.967	0.901	0.755	0.521	0.314	0.119
	0.5	0.959	0.880	0.742	0.526	0.307	0.110
	1.0	0.927	0.881	0.773	0.534	0.318	0.105
(3.05, 8.12)	0.25	0.977	0.939	0.796	0.590	0.396	0.196
	0.5	0.984	0.936	0.796	0.590	0.387	0.192
	1.0	0.990	0.939	0.785	0.585	0.382	0.194

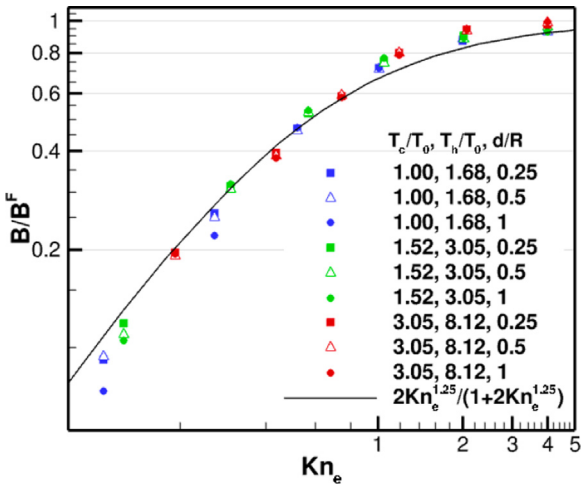

Fig. 13. (Color online) Pressures acting on the double-plate normalized by those in free molecular flow versus Kn_e for different plate temperatures and d/R.

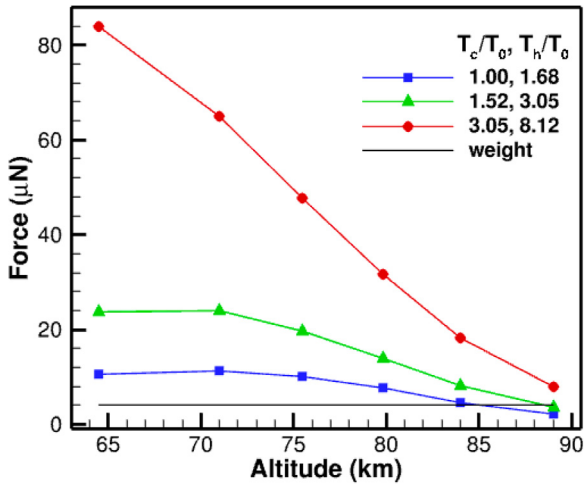

Fig. 14. (Color online) Force production versus operating altitudes for a double-plate aerostat for different plate temperatures with$R = 0.5$ cm and $d = 0.125$ cm. Dark line: gravitational force of the double-plate with an areal density of $2.7\mathrm{g}\cdot\mathrm{m}^{-2}$ for each pate.

temperatures. The dark solid lines in the figures are the weights of the double-plate with areal densities of 2.7 $\mathrm{g}\cdot\mathrm{m}^{-2}$, which corresponds to the thinnest film material that has been used for balloons. Comparing the propulsive and gravitational forces, it is evident that the double-plate with $R = 0.5$ cm and $d = 0.125$ cm could lift itself in the altitude range of 65–83 km when the plate temperatures were $T_c/T_0 = 1$ and $T_h/T_0 = 1.68$. For higher plate temperatures, such as $T_c/T_0 = 1.52$ and $T_h/T_0 = 3.05$, the double-plate could lift itself to an altitude of 88 km.

4.4. Heat flux towards the plates

The heat flux towards the plates transferred by gas can be calculated by the energy exchange of the incident and reflected molecules. The heat fluxes toward the surfaces in free molecular flow, which can be obtained according to Eq. (9), are listed in Tab. 3.

It can be seen that the heat fluxes toward the surfaces are negative because of the higher surface temperature than the environment except for the "c.l." surfaces. When the gap distance is small, molecules impinging on the lower surface of the colder plate mostly come from the upper surface of the hotter plate, which results in a positive heat flux towards the surface and the colder plate. Table 3 shows that the turning points of gap distances for the energy flux towards the colder plate for $(T_c/T_0, T_h/T_0) = (1.52, 3.05), (3.05, 8.12)$ locate at a d/R between 0.5 and 1.

Fig. 15 displays variations of the normalized heat flux towards each plate with Knudsen number. It is shown in Fig. 15(a) that the heat flux toward the hotter plate decreases with decreasing Knudsen number and increasing gap distances. The influence of the plate temperatures on the value of H_h/H_h^F has two sides. On one side, higher plate temperatures could expand the gas around the plates, thus result in a larger local Knudsen number and larger H_h/H_h^F; on the other hand, the higher plate temperatures could result in larger downward velocity and reduces the energy exchange between the gas and the lower surface of the hotter plate. The latter effect is more important than the former for larger Knudsen numbers and smaller gap distances, therefore, the value of H_h/H_h^F for $(T_c/T_0, T_h/T_0) = (3.05, 8.12)$ is smaller than that for $(T_c/T_0, T_h/T_0) = (1, 1.52)$ when Kn equals to 0.25 or0.5; however, when Kn reduces to 0.1 and d/R equals to 1, H_h/H_h^F for $(T_c/T_0, T_h/T_0) = (3.05, 8.12)$ is 6.9% larger than that for $(T_c/T_0, T_h/T_0) = (1, 1.68)$. Fig. 15(b) shows that the influence of the Knudsen number on normalized heat flux on the colder plate depends on the gap-to-radius ratio and plate temperatures. Because magnitude of $H_{c.l.}$ decays much more slowly with decreasing Kn than $H_{c.u.}$, the importance of the positive $H_{c.l.}$ increases with decreasing Kn. As a result, H_c/H_c^F could increase with dcreasing Kn if H_c^F is positive, such as for $d/R = 0.5$ and plate temperatures of $(T_c/T_0, T_h/T_0) = (1.52, 3.05)$, $(3.05, 8.12)$; H_c/H_c^F could be negative for small Knudsen numbers when H_c^F is negative, such as for $d/R = 1$ and $(T_c/T_0, T_h/T_0) = (1.52, 3.05)$.

Even though the plate temperature and gap distance have great influences on the normalized heat flux toward each plate, their influence on the normalized heat flux on the double-plate is weak, as displayed in Fig. 16. The gap distance caused a deviation which is smaller than 5.8% of H/H^F for all the studied cases. When $Kn \geq 0.25$, the influence of plate tempeartures on H/H^F is smaller than 2.7%, when $Kn = 0.1$, the value of H/H^F for $(T_c/T_0, T_h/T_0) = (3.05, 8.12)$ could be 16% larger than that for

Table 3
The heat fluxes ($W\cdot\mathrm{m}^{-2}$) acting on the plate surfaces for free molecular flow in conditions of various gap distances and plate temperatures.

$\left(\frac{T_c}{T_0}, \frac{T_h}{T_0}\right)$	d/R	H^F	H_h^F	H_c^F	$H_{h.l.}^F$	$H_{h.u.}^F$	$H_{c.l.}^F$	$H_{c.u.}^F$
	0.25	−165.3	−270.8	105.6	−135.4	−135.4	105.6	0
(1, 1.68)	0.5	−188.3	−270.8	82.61	−135.4	−135.4	82.61	0
	1	−219.2	−270.8	51.81	−135.4	−135.4	51.81	0
	0.25	−624.8	−735.9	111.1	−408.3	−327.6	214.7	−103.6
(1.52, 3.05)	0.5	−711.5	−753.4	41.9	−408.3	−345.1	145.5	−103.6
	1	−827.9	−777.0	−50.97	−408.3	−368.7	52.63	−103.6
	0.25	−2229	−2518	288.8	−1418	−1100	697.1	−408.3
(3.05, 8.12)	0.5	−2539	−2587	48.4	−1418	−1169	456.7	−408.3
	1	−2954	−2680	−274.1	−1418	−1262	134.2	−408.3

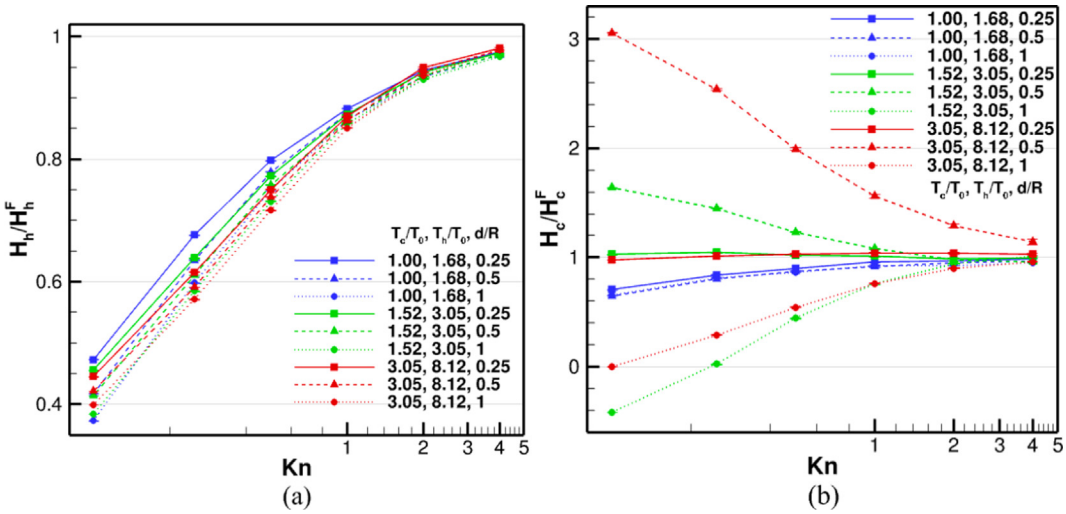

Fig. 15. (Color online) Normalized heat flux towards the hotter plate (a) and colder plate (b) versus Knudsen number for different plate temperatures and gap distances.

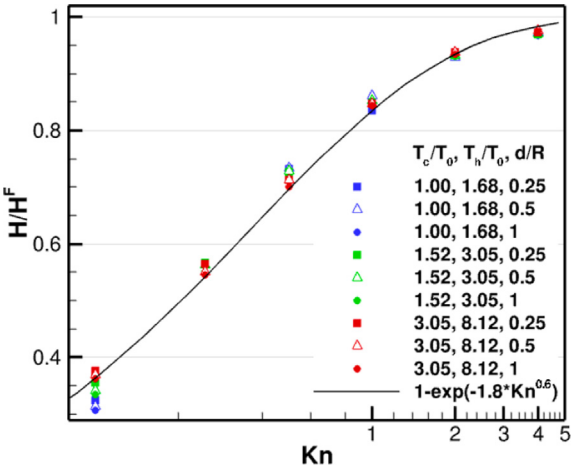

Fig. 16. (Color online) Normalized heat flux towards the double-plate versus Knudsen number for different plate temperatures and gap distances.

$(T_c/T_0, T_h/T_0) = (1, 1.68)$. Fig. 15 demonstrates that the heat flux towards the double-plate could be well fitted by $H/H^F = 1 - \exp(-1.8Kn^{0.6})$ for the range of Kn in this work.

5. Conclusions

The rarefied flow around a double-plate was studied in this work. The two parallel plates act repulsively toward each other, therefore, they could be linked by flexible materials. Kinetical analyses reveal that the influences of gap distance on the force and heat flux in free molecular flow for $d/R < 2$ can be well described by $B^F/B_0^F = \exp(-0.724d/R)$ and $H^F/H_0^F = 2 - \exp(-d/R)$ respecitvely. By combining dimensional analyses with numerical simulations, dependences of the flow field, pressure distributions, force production and heat flux on Kn, the gap-to radius ratio and the plate temperatures were analyzed. The pressure distributions acting on the plates along the axial direction showed that the magnitude of the pressure was larger in the central region than on the edge for moderate gap distances and large Knudsen numbers; however, for small Knudsen numbers and gap distances, the maximum pressure acting on the plates was located at a distance that depended on the gap distance away from the edge. Furthermore, interactions between the downward mainstream and the double-plate could result in a downward pressure acting on the edge of the double-plate for very small Knudsen numbers. The influence of the plate temperatures on the gas dynamics can be explained by the by the stronger expansion effect and larger local Kn for higher plate temperature. The influence of the gap-to radius ratio on the normalized force was small for the range of Kn studied in this work. An analytical formulation was developed to calculate the force acting on the double-plate for the range of Kn studied in this work. Applying the results to a specific double-plate, we found that the double-plate could produce a force which is larger than its weight at altitudes around 70 km when the parameters were properly selected. Though the gap distance imposes a great influence on the normalized heat flux for each plate, its influence on that for the double-plate is much weaker. The normalized heat flux acting on the double-plate could be well approximated by $H/H^F = 1 - \exp(-1.8Kn^{0.6})$ for the range of Kn and gap-to-radius ratio in this work. This work could be useful for understanding the flow around the double-plate and applying the radiometric phenomena to space technology.

Declaration of Competing Interest

The authors declare that they have no known competing financial interests or personal relationships that could have appeared to influence the work reported in this paper.

Acknowledgements

This work was supported by the Strategic Priority Research Program of Chinese Academy of Sciences (Grant No. XDA17020102) and the Youth Fund of State Key Laboratory of High Temperature Gas Dynamics (Grant No. QN20210012).

References

Akhlaghi, H., Roohi, E., 2013. Mass flow rate prediction of pressure-temperature-driven gas flows through micro/nanoscale channels. Continuum Mech. Thermodynam. 26 (1), 67–78.

Andrew, S., Aaron, P., Borges, S. I., et al., 2017. Microscale in-Plane Knudsen Radiometric Actuator: Design, Characterization, and Performance Modeling. J. Microelectromech. S. 26, 528–538.

Anikin, Y.A., 2011. Numerical study of the radiometric phenomenon exhibited by a rotating crookes radiometer. Comp. Math. Math. Phys. 51 (11), 1923–1932.

Baier, T., Hardt, S., Shahabi, V., et al., 2017. Knudsen pump inspired by crooks radiometer with a specular wall. Phys. Rev. Fluids 2 033401.

Barzegar Gerdroodbary, M., Ganji, D.D., Taeibi-Rahni, M., Vakilipour, S., 2017. Effect of knudsen thermal force on the performance of low-pressure micro gas sensor. Eur. Phys. J. Plus 132 (7). https://doi.org/10.1140/epjp/i2017-11587-4.

Barzegar Gerdroodbary, M., Ganji, D.D., Shiryanpour, I., Moradi, R., 2018a. Mass analysis of CH4/SO2 gas mixture by low-pressure mems gas sensor. J. Nat. Gas. Sci. Eng. 53, 317–328.

Barzegar Gerdroodbary, M., Ganji, D.D., Taeibi-Rahni, M., Vakilipour, S., 2018b. Effect of geometrical parameters on radiometric force in low-pressure mems gas actuator. Microsyst. Technol. 24 (5), 2189–2198.

Benford, G., Benford, J., 2005. An aero-spacecraft for the far upper atmosphere supported by microwaves. Acta Astronaut. 56 (5), 529–535.

Bird, G.A., 1994. Molecular Gas Dynamics and the Direct Simulation of Gas Flows. Clarendon Press, Oxford.

Chen, S., Xu, K., Lee, C., 2012. The dynamic mechanism of a moving crookes radiometer. Phys. Fluids 24 (11), 111701. https://doi.org/10.1063/1.4765353.

Cornella, B. M., Ketsdever, A. D., Gimelshein, N. E., et al. 2011 Impact of Separation Distance on Multi-Vane Radiometer Configurations.

Cornella, B.M., Ketsdever, A.D., Gimelshein, N.E., Gimelshein, S.F., 2012. Analysis of multivane radiometer arrays in high-altitude propulsion. J Propul. Power 28 (4), 831–839.

Crookes, W., 1874. XV. On attraction and repulsion resulting from radiation. Phil. Trans. R. Soc. Lond. A 164, 501–527.

Donkov, A.A., Tiwari, S., Liang, T., Hardt, S., Klar, A., Ye, W., 2011. Momentum and mass fluxes in a gas confined between periodically structured surfaces at different temperatures. Phys. Rev. E 84 (1). https://doi.org/10.1103/PhysRevE.84.016304.

Duermann, C., Wurm, G., Kuepper, M., 2013. Radiative forces on macroscopic porous bodies in protoplanetary disks: laboratory experiments. Astron. Astrophys. 558, A70. https://doi.org/10.1051/0004-6361/201321365.

Firuzi, S., Gong, S., 2018. Attitude Control of a Flexible Solar Sail in Low Earth Orbit. J. Guid. Control Dynam. 41 (8), 1715–1730.

Goshayeshi, B., Roohi, E., Stefanov, S., 2015. Dsmc Simulation of Hypersonic Flows Using an Improved Sbt-Tas Technique. J. Comp. Phys. 303, 28–44.

Hassanvand, A., Gerdroodbary, M.B., Moradi, R., Amini, Y., 2018. Application of Knudsen Thermal Force for Detection of Inert Gases. Results in Phys. 9, 351–358.

Ketsdever, A., Gimelshein, N., Gimelshein, S., Selden, N., 2012. Radiometric Phenomena: From the 19th to the 21st Century. Vacuum 86 (11), 1644–1662.

Küpper, M., Dürmann, C., de Beule, C., Wurm, G., 2014. Propulsion of Porous Plates in Thin Atmospheres by Temperature Fields. Microgravity Sci. Tec. 25 (5), 311–318.

Lotfian, A., Roohi, E., 2019. Radiometric Flow in Periodically Patterned Channels: Fluid Physics and Improved Configurations. J. Fluid Mech. 860, 544–576.

Lotfian, A., Roohi, E., 2021. Binary Gas Mixtures Separation Using Microscale Radiometric Pumps. Int. Commun. Heat Mass 121, 105061. https://doi.org/10.1016/j.icheatmasstransfer.2020.105061.

Lu, Z., 2005. Experimental and Numerical Study of the Optimal Operation Pressure within Crookes Radiometer. J. Vac. Sci. Technol. A 23 (6), 1531–1534.

Nallapu, R.,Tallapragada, A.,Thangavalautham, J. 2017 Radiometric Actuators for Spacecraft Attitude Control.

National Oceanic and Atmospheric Administration, National Aeronautics and Space Administration, United States Air Force. U. S. Standard Atmosphere. Washington, D.C 1976.

Passian, A., Warmack, R.J., Ferrell, T.L., Thundat, T., 2003. Thermal Transpiration at the Microscale: A Crookes Cantilever. Phys. Rev. Lett. 90 (12). https://doi.org/10.1103/PhysRevLett.90.124503.

Pikus, A., Sebastião, I.B., Strongrich, A., et al., 2019. Characterization of a Knudsen Force Based Vacuum Sensor for N2/H2O Gas Mixtures. Vacuum 161, 130–137.

Rainwater, E. L., Fairbrother, D., Smith, M. November 2003 Extended Capabilities of Zero-Pressure and Superpressure Scientific Ballooning Platforms.

Rainwater, E.L., Smith, M.S., 2004. Ultra High Altitude Balloons for Medium-to-Large Payloads. Adv. Space Res. 33 (10), 1648–1652.

Roohi, E., Darbandi, M., 2012. Recommendations on Performance of Parallel Dsmc Algorithm in Solving Subsonic Nanoflows. Appl. Math. Model. 36 (5), 2314–2321.

Roohi, E., Stefanov, S., 2016. Collision Partner Selection Schemes in Dsmc: From Micro/Nano Flows to Hypersonic Flows. Phys. Rep. 656, 1–38.

Scandurra, M., Iacopetti, F., Colona, P., 2007. Gas kinetic forces on thin plates in the presence of thermal gradients. Phys. Rev. E Stat. Nonlin. Soft Matter Phys. 75 (2). https://doi.org/10.1103/PhysRevE.75.026308.

Selden, N., Ngalande, C., Gimelshein, N., Gimelshein, S., Ketsdever, A., 2009a. Origins of radiometric forces on a circular vane with a temperature gradient. J. Fluid Mech. 634, 419. https://doi.org/10.1017/S0022112009007976.

Selden, N., Ngalande, C., Gimelshein, S., Muntz, E.P., Alexeenko, A., Ketsdever, A., 2009b. Area and edge effects in radiometric forces. Phys. Rev. E 79 (4). https://doi.org/10.1103/PhysRevE.79.041201.

Shahabi, V., Baier, T., Roohi, E., et al., 2017. Thermally induced gas flows in ratchet channels with diffuse and specular boundaries. Sci. Rep. 7 (1), 1–14.

Sharipov, F., Seleznev, V., 1998. Data on internal rarefied gas flows. J. Phys. Chem. Ref. Data 27 (3), 657–706.

Sista, S.V., Bhattacharya, E., 2014. Knudsen force based mems structures. J. Micromech. Microeng. 24 (4), 045003. https://doi.org/10.1088/0960-1317/24/4/045003.

Sone, Y., 2000. Flows induced by temperature fields in a rarefied gas and their ghost effect on the behavior of a gas in the continuum limit. Annu. Rev. Fluid Mech. 32 (1), 779–811.

Stanhill, G., 2019. Sir william crookes and his radiometer. Weather 74 (2), 56–57.

Strongrich, A., Alexeenko, A., 2015. Microstructure Actuation and Gas Sensing by the Knudsen Thermal Force. Appl. Phys. Lett. 107 (19), 193508. https://doi.org/10.1063/1.4935461.

Taguchi, S., Aoki, K., 2012. Rarefied gas flow around a sharp edge induced by a temperature field. J. Fluid Mech. 694, 191–224.

Taguchi, S., Aoki, K., 2015. Motion of an Array of Plates in a Rarefied Gas Caused by Radiometric Force. Phys Rev E Stat Nonlin Soft Matter Phys 91(6), 063007. "Ultra-Thin-Film Balloon Reached the Highest Altitude." http://www.isas.ac.jp/e/snews/2002/06_02.shtml.

Ventura, A., Gimelshein, N., Gimelshein, S., Ketsdever, A., 2013. Effect of vane thickness on radiometric force. J. Fluid Mech. 735, 684–704.

Wang, X., Zhang, Z., Zhang, W., Zhang, P., Zhang, S., 2019. Numerical simulation of thermal edge flow in ratchet-like periodically patterned micro-channels. Int. J. Heat Mass Transf. 135, 1023–1038.

White, C., Colombo, C., Scanlon, T.J., McInnes, C.R., Reese, J.M., 2013. Rarefied gas effects on the aerodynamics of high area to mass ratio spacecraft in orbit. Adv. Space Res. 51 (11), 2112–2124.

Wolfe, D., Larraza, A., Garcia, A., 2016. A horizontal vane radiometer experiment, theory, and simulation. Phys. Fluids 28 (3), 037103. https://doi.org/10.1063/1.4943543.

Zeng, D., Cai, R., Yang, Y., 2020. Dsmc study of the radiometric force acting on a thin plate with surface temperatures much higher than the environment temperature. Int. J. Mech. Sci. 187, 105922. https://doi.org/10.1016/j.ijmecsci.2020.105922.

Zhu, L., Guo, Z., 2017. Numerical study of nonequilibrium gas flow in a microchannel with a ratchet surface. Phys. Rev. E 95 (2). https://doi.org/10.1103/PhysRevE.95.023113.